Evaluation of the dielectric function of colloidal $Cd_{1-x}Hg_xTe$ quantum dot films by spectroscopic ellipsometry

A. Bejaoui[1], M. I. Alonso[2], M. Garriga[2], M. Campoy-Quiles[2], A. R. Goñi[2,3], F. Hetsch[1], S. V. Kershaw[1], A. L. Rogach[1], C. H. To[1], Y. Foo[1], J.A. Zapien[1]

[1] Department of Physics and Materials Science and Centre for Functional Photonics (CFP), City University of Hong Kong, Hong Kong SAR

[2] Institut de Ciència de Materials de Barcelona, ICMAB-CSIC, Campus de la UAB, 08193 Bellaterra, Spain

[3] ICREA, Passeig Lluís Companys 23, 08010 Barcelona, Spain

Abstract:

We report on the investigation by spectroscopic ellipsometry of films containing $Cd_{1-x}Hg_xTe$ alloy quantum dots (QDs). The alloy QDs were fabricated from colloidal CdTe QDs grown by an aqueous synthesis process followed by an ion-exchange step in which Hg^{2+} ions progressively replace Cd^{2+}. For ellipsometric studies, several films were prepared on glass substrates using layer-by-layer (LBL) deposition. The contribution of the QDs to the measured ellipsometric spectra is extracted from a multi-sample, transmission and multi- angle-of-incidence ellipsometric data analysis fitted using standard multilayer and effective medium models that include surface roughness effects, modeled by an effective medium approximation. The relationship of the dielectric function of the QDs retrieved from these studies to that of the corresponding II-VI bulk material counterparts is presented and discussed.

Key words:

$Cd_{1-x}Hg_xTe$, colloidal quantum dots, spectroscopic ellipsometry, ion exchange, dielectric function.

1. Introduction:

$Cd_{1-x}Hg_xTe$ quantum dots (QDs) are semiconducting nanocrystals that have attracted widespread attention owing to their distinct optical and electronic properties. QDs are quasi-spherical crystals with maximum radii of a few nanometers, in which the spacing and density of the energy levels available for electron occupation become highly dependent on the dimensions of the particle because of quantum size effects [1]. Well controlled synthesis methods, such as hydrothermal growth [2-5], allow for the production of large quantities of QDs with narrow size distributions in which the average nanocrystal radii are chosen by varying the synthesis duration. The resulting QDs therefore present tunable absorption peak positions, narrow emission spectra and long lifetimes [4] that may be tailored to a variety of uses, such as biological applications [6], photovoltaic devices [7], and light-emitting diode (LED) display applications [8].

Many photometric studies of QDs have been carried out [9,10], allowing for the collection of spectrally resolved absorption and emission information, however, only few optical studies of the complex dielectric function of QDs using spectroscopic ellipsometry (SE) have been reported, for instance HgTe [11], CdTe [12], Si [13] and Ge [14] QDs. The dielectric function information is essential to understand the interaction of QDs with light and thereby predict and optimize the optical behavior and performance of QD-based devices. SE can reveal detailed information about transitions at higher energies, rather than simply the energy gap associated with the band edge transition most often extracted from regular absorption spectroscopy. For example, accurate knowledge of the QD dielectric function is a basic requirement for device rationalization and optimization in nanowire-based solar cells where QDs are being used as sensitizers (QDSC) [15,16]. In such applications, not only the expected groundbreaking performance has not been materialized but, in fact, detailed knowledge of their operation remains elusive [15,16]. A clear example is the poor performance, compared to the TiO nanoparticle, of ZnO nanorod/nanowire scaffolding sensitized with QDSCs despite ZnO having higher electron mobility, enhanced charge collection, and better electron injection kinetics [16-19]. In addition, light trapping in nanostructures is thought to have the potential to overcome the Yablonovitch and Cody limit [20-24].

Studies of the complex dielectric function of QD materials are severely limited as in most cases they relate to absorption measurements usually reported in arbitrary units. For example, in the case of CdSe QDs, one of the most widely studied QD materials, published (*n*, *k*) data is restricted to QDs with ~4 nm diameter [25]; and even in this case (*n*, *k*) values are available only over a limited (450-800 nm) spectral range while the corresponding NIR absorption tail extends much further than expected for direct gap absorption CdSe QDs [26,27].

This work focuses on ternary alloy $Cd_{1-x}Hg_xTe$ QDs produced by an ion-exchange process in which Hg^{2+} replace progressively Cd^{2+} ions, with strong emissions [28] and long lifetimes [29] as well as the tunable emission and absorption behavior typical of QDs. This system may offer great potential for light-emitting device (LED) display applications, optoelectronics, solar cells and photovoltaic uses [30]. In many of these applications there is great potential to enhance performance by taking advantage of carrier multiplication effects under so called hot excitation conditions. In particular the initial excess photon energy could be translated into one or more additional excitons by the process of exciton fission or multiple exciton generation. Whilst the precise mechanisms (there may be several [31]) by which this multiplication process can occur in QDs remains the subject of much research work, one approach is simply to mimic the favorable conditions already known to promote multiplication in bulk materials. In some bulk $Cd_{1-x}Hg_xTe$ alloy avalanche photodiode designs [32], advantage is taken of a resonant alignment of the bandgap transition energy with the energy gap between the split-off and the degenerate light and heavy hole valence bands such that (transition energy) conditions for the split-off band inverse Auger process [33] (also referred to as an impact ionization process) are engineered to be especially favorable. In order to be able to do similar transition energy engineering in QDs it is therefore necessary to determine both the composition and size effects on the bandgap energy and on the spin orbit transition between the split-off and degenerate light and heavy hole levels [12] so that the two can be closely tailored (by adjusting the composition) after taking account of the effect of quantum confinement [34].

We have determined the optical properties of $Cd_{1-x}Hg_xTe$ QDs in the 250-1700 nm spectral range by spectroscopic ellipsometry (SE) measured in QD films prepared by layer-by-layer (LBL) deposition on glass substrates. In addition, the morphology and surface roughness of the prepared films is evaluated by SE using an effective medium approximation (EMA), being in

good agreement with complementary surface characterization by atomic force microscopy (AFM).

2. Experimental details

Synthesis of $Cd_{1-x}Hg_xTe$ alloy colloidal QDs: The $Cd_{1-x}Hg_xTe$ QDs were formed by chemical modification of CdTe QDs through exchange between Hg^{2+} and Cd^{2+} ions [35]. The CdTe QD starting material (2.3 nm diameter) with a cubic zinc blende crystal structure was synthesized and stabilized as previously reported [36,37] and then, Hg^{2+} ions were added to the CdTe colloidal solutions at a fixed pH = 11. Additional mercaptopropionic acid ligand was present in the added Hg^{2+} ion solution to solubilize the ions at high pH. In practice the relative amount of Hg^{2+} actually exchanged differed from the proportion added to the solution, and for higher Hg^{2+} doses the final Hg content was significantly lower than the ratio added in solution, as reviewed by Gupta et al.[10].

Deposition of $Cd_{1-x}Hg_xTe$ QD thin films: In this work, we used a previously reported [38-43] layer-by-layer (LBL) assembly method to deposit multilayer films. Firstly, glass substrates were thoroughly cleaned by ultrasonication in methanol, acetone and methanol, each for 15 min, then the slides were rinsed with 2-propanol and water and finally dried with N_2. In order to deposit a $Cd_{1-x}Hg_xTe$ QD thin film, the clean glass substrate was first dipped into polyethylenimine (PEI) solution in water for 10 minutes. The substrate was then washed in deionized water for 2 min, followed by a 10 min dip into the $Cd_{1-x}Hg_xTe$ QDs solution. In the final step, the sample was washed in deionized water for 2 min and dried in air. The described process forms a single layer film and in order to deposit thicker films the process was repeated. The drying step was conducted at the end rather than in every cycle of deposition. In this work, we prepared four films by performing 1, 2, 4 and 8 cycles.

Sample Characterization:

Figure 1 shows the absorption and photoluminescence spectra of the obtained $Cd_{1-x}Hg_xTe$ QDs compared to the starting CdTe QDs. Both the absorption excitonic peak position and the luminescence emission maximum shift to longer wavelength due to the exchange of Cd by Hg.

Assuming that the QD size remains constant, we ascribe the observed shift to alloying. Taking as reference the dependence at room temperature of the bandgap on composition for bulk alloys [44], the observed red shift of 0.81 eV corresponds to a relative concentration of mercury of 42%. This assumes that as in bulk $Cd_{1-x}Hg_xTe$ alloys there is no, or very little optical bowing. Since the alloy QD peak width indicates some compositional inhomogeneity (alloy fractional widths given by the FWHM/peak wavelength ratio exceed those of the CdTe starting QDs), we estimate that the inhomogeneous broadening of the alloy QD peak is caused by a composition fluctuation close to ±10%.

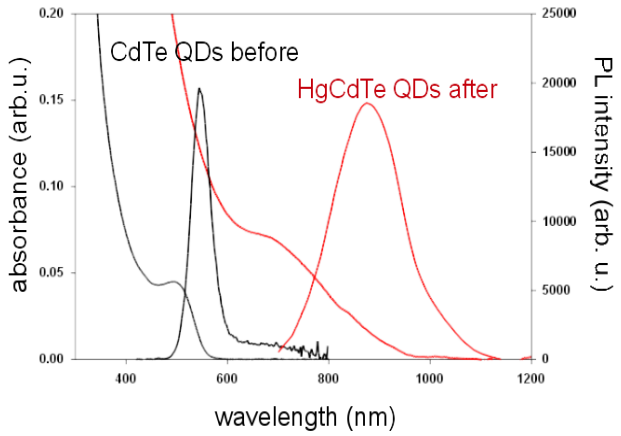

Figure 1. Optical absorption and room temperature photoluminescence (PL) spectra for CdTe and $Cd_{1-x}Hg_xTe$ QD solutions.

The structural characterization of the films was performed by Atomic Force Microscopy (AFM) using a Digital Instruments Nanoscope IV in tapping mode with a silicon tip coated with Al, force constant of 40 N/m and a resonant frequency of 300 kHz. We evaluated both the film thicknesses and surface roughness. The AFM investigation of the samples showed that the thickness increase was not linear with the number of deposition cycles. The surface roughness values also increased superlinearly. Figure 2 shows the AFM characterization of the thickest and roughest 8-cycles film. The values for all samples are listed in Table 1 together with the structural values that fit the optical data.

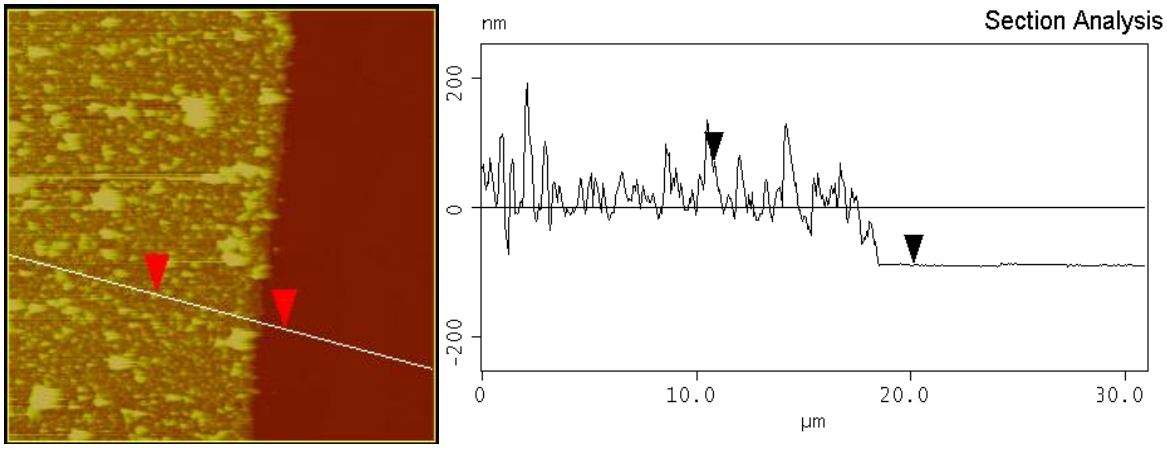

Figure 2. Atomic Force Microscopy characterization of a LBL assembled film of CdHgTe nanoparticles with 8 deposition cycles on glass substrate. The left image shows a 30x30 µm² region and, on the right panel, the profile along the marked line allows for evaluation of the average film thickness and roughness which in this case are 107.3 nm and 32.9 nm, respectively.

Table 1. Structural parameters, surface roughness and bulk film thickness, determined from AFM and SE. The quoted error bars of SE parameters are estimated from the fitting process.

Sample	Surface roughness (nm)		Film thickness (nm)	
	AFM	SE	AFM	SE
1 cycle	1.3	1.3 (fixed)	3.5	3.4±0.1
2 cycles	2.8	3.9±0.1	11.8	13.9±0.1
4 cycles	8.0	4.9±0.1	27.9	32.8±0.2
8 cycles	32.9	26.3±3.4	107.3	98.1±4.1

The optical properties of the $Cd_{1-x}Hg_xTe$ (QDs) thin films at room temperature were measured using a J. A. Woollam M2000 ellipsometer (rotating compensator type). The spectral range was between 0.7 eV and 6.5 eV. We measured transmission spectra at normal incidence as well as ellipsometry spectra at angles of incidence 55°, 60°, 65°, 70° and 75°. For modeling the SE data, both the J. A. Woollam WVASE32 software as well as in-house developed codes (Fortran and python) were used. Thickness data and roughness values obtained from AFM measurements were taken as a starting point for the model. For fitting, we used a 5 phase model consisting of the substrate, a compound layer of polymer (PEI) and $Cd_{1-x}Hg_xTe$ QDs modeled with the

effective medium approximation and air, taking into account both an intermixed layer between the substrate and the film and a roughness layer on the surface of the film.

3. Results and discussion

The dielectric function of the $Cd_{1-x}Hg_xTe$ QDs was evaluated from the transmission and spectroscopic ellipsometry data by multi-sample analysis including the SE spectra measured at five angles of incidence. This procedure can provide sufficient information to identify a unique solution that describes optical properties in complex samples [45]. As already mentioned, the structural parameters obtained from AFM measurements were taken into account to describe the optical measurements but they were treated as fitting parameters except in a few cases, as explained below.

In a first step, the optical constants of the employed glass substrate were determined by simultaneous fitting of the transmission and ellipsometry data. We also determined the optical constants of PEI by depositing a PEI-only film. These optical constants were fixed for the subsequent analysis. Then, the data measured for the four samples (with 1, 2, 4, and 8 deposition cycles) were analyzed together. In this procedure, several identical models -one for each sample- were defined with coupled optical properties for the unknown QDs dielectric function, then all data were fitted simultaneously. As already anticipated, the models consisted of 5 phases: the already known glass substrate, an EMA layer of 2 nm thickness (glass roughness determined by AFM) to represent the intermixing of glass and the film, the film, a surface roughness and the ambient (air). The roughness of the 1-cycle film was also fixed to the AFM value of 1.3 nm, whereas its thickness, as well as the thickness and roughness of 2-, 4-, and 8- cycle films, were left as fitting parameters. The surface roughness was modelled in the standard way using an EMA with 50% void volume fraction and 50% contribution from the effective dielectric function of the film. The outcome of this analysis was the dielectric function of the films and the thickness of the film and surface roughness layer.

Since a numerical point-by-point analysis was too unstable, we run the fits using parameterizations of the unknown film dielectric function. We used both a numerical approach using spline parameterizations [46] and, subsequently, a more physical model with standard

critical-point lineshapes to parameterize several observed interband transitions that will be discussed below. Both fitting approaches gave almost identical results in terms of quality of the fits. The structural values obtained from SE are quoted in Table 1 and the fitted curves are shown in Figs. 3 and 4. After this fitting process we obtained an effective film dielectric function that corresponds to the QDS/PEI composite. It is not surprising that the largest deviations from the model, especially in Fig. 3, are observed for the thickest sample which has a large roughness and for which the proposed structural model is probably too simplistic. Still, the common model describes rather well all samples.

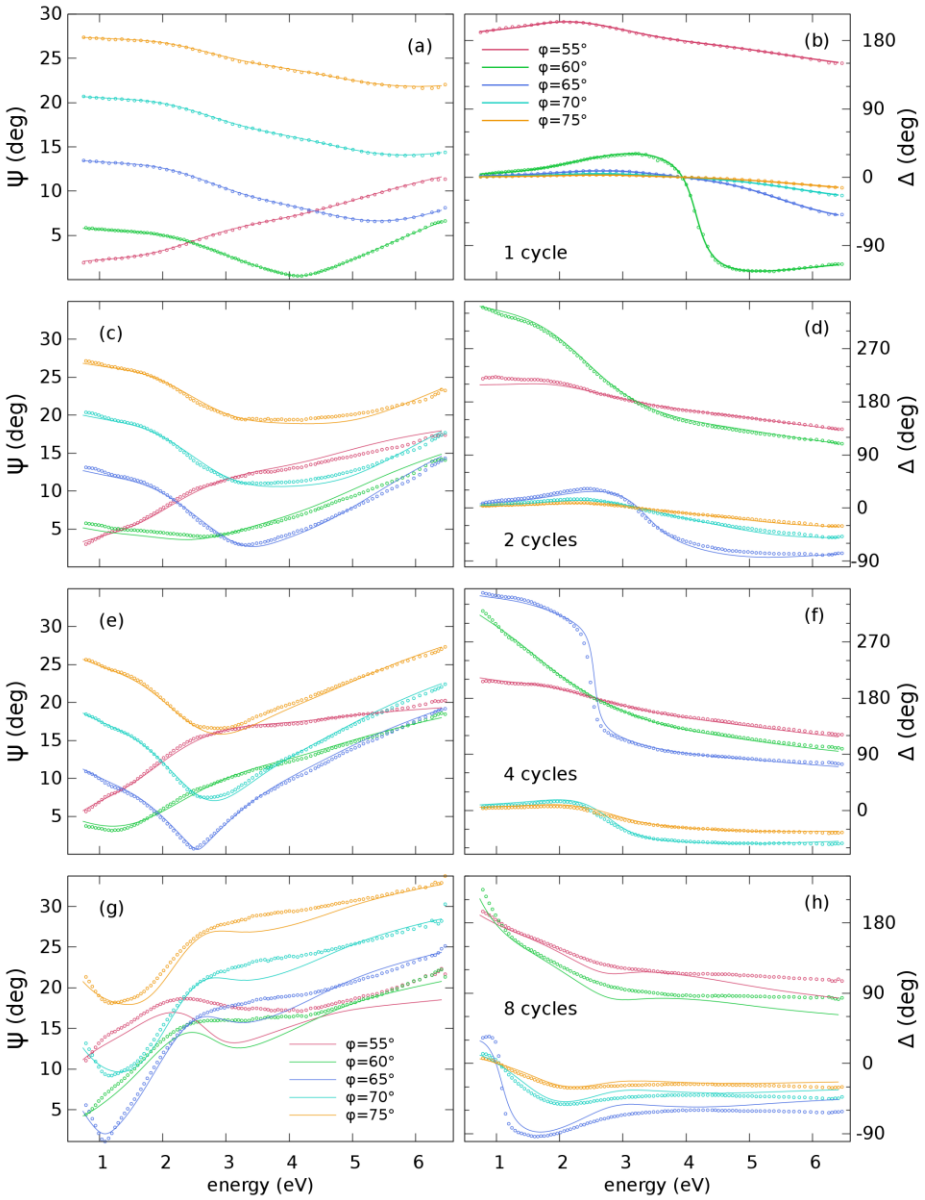

Figure 3. Spectroscopic ellipsometry parameters (ψ, Δ) showing the experimental data (circles) and best fit model (solid lines) for the 1 cycle (a) and (b), 2 cycles (c) and (d), 4 cycles (e) and (f), and 8 cycles (g) and (h). The density of plotted experimental points has been reduced for clarity. The best model was obtained by multi-sample, multi angle-of-incidence fitting to all ellipsometric and transmission (Fig. 4) data.

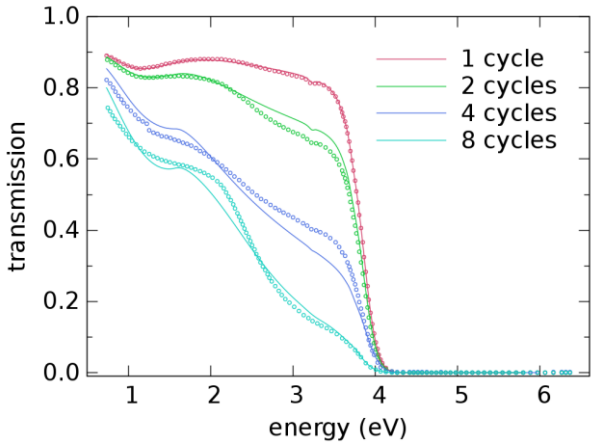

Figure 4. Transmission for HgCdTe films prepared by LBL deposition with 1, 2, 4, and 8 deposition cycles including the measured (symbols) and best fit (lines) data. The density of plotted experimental points has been reduced for clarity.

In order to obtain the absolute values of the real and imaginary parts of the dielectric function of the QDs we have to take into account that these values depend on the relative amount of QDs and PEI in the film [47]. For this purpose, the effective film dielectric function was modeled as an EMA consisting of the known PEI dielectric function and the to-be-determined contribution from the QD dielectric function. The relative volume fraction of QDs in the film is difficult to know. The mass loading of deposited material could in principle be determined by including a quartz microbalance sensor alongside the coated slides. To make the mass measurements the dipping process had to be paused and the film had to be dried out. The ratio in frequency step from the quartz crystal was about 5—10:1, which for a 8:1 ratio in QD:polymer densities would mean that the relative volume fraction of QDs in the film should be approximately near 50%. We assumed this value and the optical constants obtained for the $Cd_{0.58}Hg_{0.42}Te$ QDs in this way are plotted in Fig. 5, in which the result for a 50% relative volume fraction of QDs in the film is represented as the thicker curves in Fig. 5. A variation of ±10% is also represented in the figure as thinner lines. The higher absolute value of the dielectric function of the QD component obtains for the larger PEI amount, to compensate for the much lower refractive index of PEI in its contribution to the effective film function. Since it is difficult to know which the precise fraction is, the presented absolute value should be still regarded as approximate, probably within the given bounds.

Independently of the absolute value of the dielectric function, the observed features (inflexions and turning points) arise from the QDs because PEI is transparent in this range. We observe three interband transitions which are related to the corresponding interband transitions of bulk alloys [48]: the fundamental gap transition E_0, and the upper transitions E_1 (at the L point) and E_2 (at the X point) of the zinc blende Brillouin zone. The dielectric functions for the bulk alloys of appropriate compositions plotted in Fig. 5 are calculated using a parameterized model based on literature data [49]. The E_1 transition in the bulk displays very clear spin-orbit split components [48,49] which are not resolved in the QDs. We assume that this is due to the increased broadening of these transitions and that the structure present in the QD spectrum shows the average of these two components. Although relatively broadened, the three mentioned transitions are quite well defined in the QDs and, as in similar systems [47], strongly blue-shifted by quantum confinement effects. Since the transition energies also shift with alloy composition, the figure shows the expected variation for a possible variation of ±10% in the alloy composition, where a lower Hg content also induces blue shifts in the energies. However, these are clearly smaller than the blue shifts measured in the QDs, as indicated in Fig. 5.

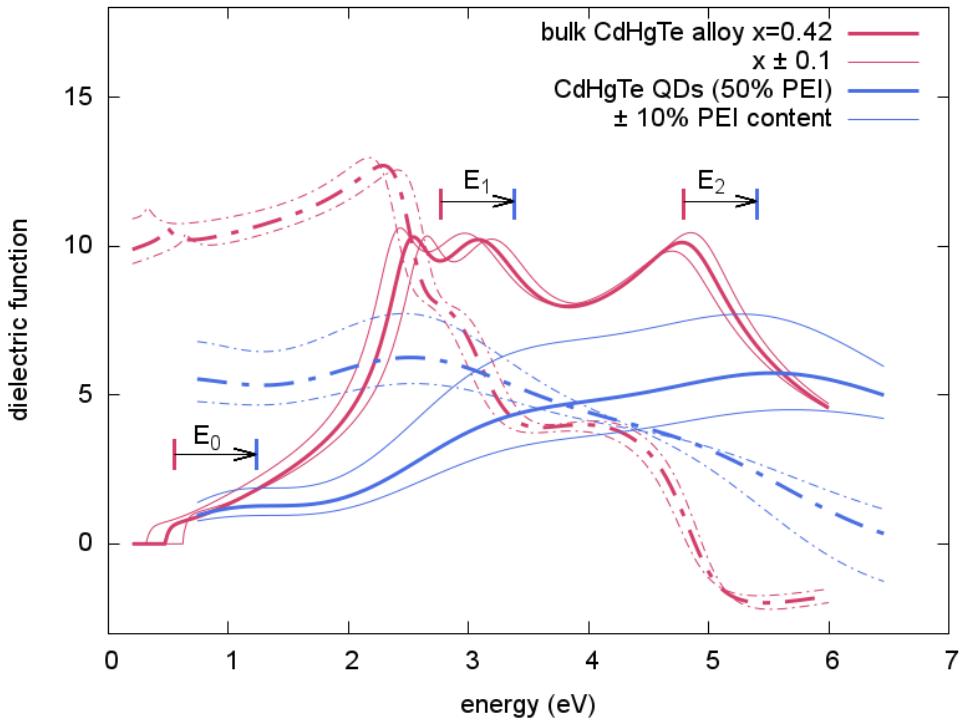

Figure 5. The dielectric function of the ternary quantum dots extracted from the optical data analysis of the prepared films (thick blue lines) as compared to that of $Cd_{0.58}Hg_{0.42}$ Te bulk reference (red curve). Solid lines display the imaginary parts and dash-dotted lines the real parts. For comparison, 10% variations in both alloy composition and in PEI content within the film are shown as thin lines. The observed blue shifts of the interband transitions E_0, E_1, and E_2 are indicated by arrows.

Conclusion:

We have obtained the optical properties of thin films prepared from $Cd_{0.58}Hg_{0.42}Te$ QDs assembled on glass substrates using layer-by-layer (LBL) deposition from successive dipping of the substrate into polyethylenimine (PEI) solution and into $Cd_{0.58}Hg_{0.42}Te$ QDs solution. An optical model was used to determine the optical properties of the QDs taking into account 1) the pre-determined optical properties of the glass substrate and PEI, and 2) the thickness and surface roughness of the films determined from AFM measurements. The simultaneous data analysis of all sample transmission spectra and multi- angle-of-incidence spectroscopic ellipsometry of films prepared with 1, 2, 4, and 8 LBL cycles enabled determination of the bulk film thickness, their surface roughness and their effective dielectric function. To avoid excessive cross-correlations of the parameters of the optical model, the surface roughness of the 1 cycle film determined from AFM was fixed, whereas all other thicknesses were fitted.

Compared to the bulk properties of $Cd_{0.58}Hg_{0.42}Te$, we found that it is possible to identify the E_0, E_1 and E_2 transition energies in the $Cd_{0.58}Hg_{0.42}Te$ QD films and observe quantum confinement related blue shifts for this alloy composition and size. Spin-orbit effects for the E_1 transition energy are particularly relevant in the design of alloy QDs with strong multiple exciton generation (MEG) quantum yields and a knowledge of the shift in the transition energies helps to design materials that may take advantage of resonant enhancement of exciton fission[34].

Acknowledgements:

The authors acknowledge financial support from the RGC/CSIC Joint Research Scheme with Refs. S-HK001/12 (RGC) and 2011HK0016 (CSIC). MIA, MG, MCQ and ARG thank the Spanish Ministry of Economy and Competitiveness for funding through grant MAT2015-70850-P, and the "Severo Ochoa" Programme for Centres of Excellence in R&D (SEV-2015-0496). JAZ acknowledges partial support from Project CityU 122812 from the Research Grants Council of Hong Kong.

References:

[1] A. P. Alivisatos, Perspectives on the physical chemistry of semiconductor nanocrystals, J. Phys. Chem. 100 (1996) 13226-13239.

[2] N. Gaponik, D. V. Talapin, A. L. Rogach, K. Hoppe, E. V. Shevchenko, A. Kornowski, A. Eychmüller, H. Weller, Thiol-capping of CdTe nanocrystals: an alternative to organometallic synthetic routes, J. Phys. Chem. B 106 (2002) 7177-7185.

[3] A. Shavel, N. Gaponik, A. Eychmüller, Factors governing the quality of aqueous CdTe nanocrystals: calculations and experiment, J. Phys. Chem. B 110 (2006) 19280-19284.

[4] N. Gaponik, A. L. Rogach, Thiol-capped CdTe nanocrystals: progress and perspectives of the related research fields, Phys. Chem. Chem. Phys. 12 (2010) 8685-8693.

[5] S. Leubner, S. Hatami, N. Esendemir, T. Lorenz, J. O. Joswig, V. Lesnyak, S. Recknagel, N. Gaponik, U. Resch-Genger, A. Eychmüller, Experimental and theoretical investigations of the ligand structure of water-soluble CdTe nanocrystals, Dalton Trans. 42 (2013) 12733-12740.

[6] P. M. Allen, W. Liu, V. P. Chauhan, J. Lee, A. Y. Ting, D. Fukumura, R. K. Jain, M. G. Bawendi, InAs(ZnCdS) quantum dots optimized for biological imaging in the near-infrared, Am. Chem. Soc. 128 (2006) 2526-2527.

[7] Z. Yang, H.-T. Chang, CdHgTe and CdTe quantum dot solar cells displaying an energy conversion efficiency exceeding 2%, Sol. Ener. Mater. Sol. Cells 94 (2010) 2046-2051.

[8] E. Jang, S. Jun, H. Jang, J. Lim, B. Kim, Y. Kim, White-light-emitting diodes with quantum dot color converters for display backlights, Adv. Mater. 22 (2010) 3076-3080.

[9] H. Qian, C. Dong, J. Peng, X. Qiu, Y. Xu, J. Ren, High-quality and water-soluble near-infrared photoluminescent CdHgTe/CdS quantum dots prepared by adjusting size and composition, J. Phys. Chem. C 111 (2007) 16852-16857.

[10] S. Gupta, S. V. Kershaw, A. L. Rogach, Ion exchange in colloidal nanocrystals, Adv. Mater 25 (2013) 6923-6944.

[11] V. Rinnerbauer, M. Kovalenko, V. Lavchiev, G. Kocher, J. Roither, W. Heiss, K. Hingerl, Spectroscopic ellipsometry of layer by layer deposited colloidal HgTe nanocrystals exhibiting quantum confinement, Physica E 32 (2006) 104-107.

[12] P. Babu Dayal, B. R. Mehta, P. D. Paulson, Spin-orbit splitting and critical point energy at Γ and L points of cubic CdTe nanoparticles: effect of size and nonspherical shape, Phys. Rev. B. 72 (2005) 115413.

[13] M. I. Alonso, I. C. Marcus, M. Garriga, A. R. Goñi, J. Jedrzejewski, I. Balberg, Evidence of quantum confinement effects on interband optical transitions in Si nanocrystals, Phys. Rev. B 82 (2010) 045302.

[14] M. I. Alonso, M. Garriga, A. Bernardi, A. R. Goñi, A. F. Lopeandia, G. Garcia, J. Rodríguez-Viejo, J. L. Lábár, Ellipsometric measurements of quantum confinement effects on higher interband transitions of Ge nanocrystals, Phys. stat. sol. (a) 205 (2008) 888-891.

[15] A. I. Hochbaum, P. Yang, Semiconductor nanowires for energy conversion, Chem. Rev. 110 (2010) 527-546.

[16] Q. Zhang, G. Cao, Nanostructured photoelectrodes for dye-sensitized solar cells, Nano Today 6 (2011) 91-109.

[17] I. Mora-Seró, J. Bisquert, Breakthroughs in the development of semiconductor-sensitized solar cells, J. Phys. Chem. Lett. 1 (2010) 3046-3052.

[18] I. Mora-Seró, S. Giménez, F. Fabregat-Santiago, R. G. Gómez, Q. Shen, T. Toyoda, J. Bisquert, Recombination in quantum dot sensitized solar cells, Acc. Chem. Res. 42 (2009) 1848-1857.

[19] S. Rühle, M. Shalom, A. Zaban, Quantum-dot-sensitized solar cells, Chem. Phys. Chem 11 (2010) 2290-2304.

[20] Z. P. Yang, L. Ci, J. A. Bur, S. Y. Lin, P. M. Ajayan, Experimental observation of an extremely dark material made by a low-density nanotube array, Nano Lett. 8 (2008) 446-451.

[21] K. R. Catchpole, S. Mokkapati, F. Beck, E.-C. Wang, A. McKinley, A. Basch, J. Lee, Plasmonics and nanophotonics for photovoltaics, MRS Bull. 36 (2011) 461-467.

[22] H. Alaeian, A. C. Atre, J. A. Dionne, Optimized light absorption in Si wire array solar cells, J. Opt. 14 (2012), 024006.

[23] R. Tena-Zaera, J. Elias, C. Lévy-Clément, ZnO nanowire arrays: optical scattering and sensitization to solar light, Appl. Phys. Lett. 93 (2008) 233119.

[24] E. Yablonovitch, G. D. Cody, Intensity enhancement in textured optical sheets for solar cells, IEEE Trans. Electron Devices 29 (1982) 300-305.

[25] E. Marx, D. S. Ginger, K. Walzer, K. Stokbro, N. C. Greenham, Self-Assembled monolayers of CdSe nanocrystals on doped GaAs substrates, Nano Lett. 2 (2002) 911-914.

[26] S. Neeleshwar, C. Chen, C. Tsai, Y. Chen, S. Shyu, M. Seehra, Size-dependent properties of CdSe quantum dots, Phys. Rev. B 71 (2005) 201307.

[27] S. H. Tolbert, A. B. Herhold, C. S. Johnson, A. P. Alivisatos, Comparison of quantum confinement effects on the electronic absorption spectra of direct and indirect gap semiconductor nanocystals, Phys. Rev. Lett. 73 (1994) 3266-3269.

[28] A. L. Rogach, M. T. Harrison, S. V. Kershaw, A. Kornowski, M. G. Burt, A. Eychmüller, and H. Weller, Colloidally prepared CdHgTe and HgTe quantum dots with strong near-infrared luminescence, Phys. Stat. Sol. (b) 224 (2001) 153-158.

[29] S. Gupta, O. Zhovtiuk, A. Vaneski, Y.-C. Lin, W.-C. Chou, S. V. Kershaw, A. L. Rogach, $Cd_x Hg_{(1-x)}$ Te alloy colloidal quantum dots: tuning optical properties from the visible to near-infrared by ion exchange, Part. Part. Syst. Charact. 30 (2013) 346-354.

[30] A.B.M.O. Islam, N.B. Chaure, J. Wellings, G. Tolan, I.M. Dharmadasa, Development of electrodeposited ZnTe layers as window materials in ZnTe/CdTe/CdHgTe multi-layer solar cells, Mater. Charact. 60 (2009) 160-163.

[31] A. R. Beattie, Quantum efficiency in InSb, J. Phys. Chem. Solids 23 (1962) 1049-1056.

[32] P. Norton, HgCdTe infrared detectors, Opto-Electron. Rev. 10 (2002) 159-174.

[33] A. Rogalski, Infrared Detectors, CRC Press, Boca Raton (2010).

[34] S. V. Kershaw, S. Kalytchuk, O. Zhovtiuk, Q. Shen, T. Oshima, W. Yindeesuk, T Toyoda, A. L. Rogach, Multiple exciton generation in cluster-free alloy $Cd_xHg_{1-x}Te$ colloidal quantum dots synthesized in water, Phys. Chem. Chem. Phys. 16 (2014) 25710-25722.

[35] M.T. Harrison, S.V. Kershaw, M.G. Burt, A. Eychmüller, H. Weller, A.L. Rogach, Wet chemical synthesis and spectroscopic study of CdHgTe nanocrystals with strong near-infrared luminescence, Mater. Sci. Eng. B 69-70 (2000) 355-360.

[36] A. L. Rogach, L. Katsikas, A. Kornowski, D. Su, A. Eychmuller, H. Weller, Synthesis and characterization of thiol-stabilized CdTe nanocrystals, Ber. Bunsenges. Phys. Chem. 100 (1996) 1772-1778.

[37] S. Wu, J. Dou, J. Zhang, S. Zhang, A simple and economical one-pot method to synthesize high-quality water soluble CdTe QDs, J. Mater. Chem. 22 (2012) 14573-14578.

[38] G. Decher, Fuzzy nanoassemblies: toward layered polymeric multicomposites, Science 277 (1997) 1232-1237.

[39] N. A. Kotov, I. Dekany, J. H. Fendler, Layer-by-layer self-assembly of polyelectrolyte-semiconductor nanoparticle composite films, J. Phys. Chem. 99 (1995) 13065-13069.

[40] A. L. Rogach, D. S. Koktysh, M. Harrison, N. A. Kotov, Layer-by-layer assembled films of HgTe nsnocrystals with strong infrared emission, Chem. Mater. 12 (2000) 1526-1528.

[41] M. T. Crisp, N. A. Kotov, Preparation of nanoparticle coatings on surfaces of complex geometry, Nano Lett. 3 (2003) 173-177.

[42] D. Y. Wang, A. L. Rogach, F. Caruso, Semiconductor quantum dot-labeled microsphere bioconjugates prepared by stepwise self-assembly, Nano Lett. 2 (2002) 857-861.

[43] A. Rogach, A. Susha, F. Caruso, G. Sukhorukov, A. Kornowski, S. Kershaw, H. Möhwald, A. Eychmüller, H. Weller, Nano- and microengineering: 3-D colloidal photonic crystals prepared from Sub-μm-sized polystyrene latex spheres pre-coated with luminescent polyelectrolyte/nanocrystal shells. Adv. Mater. 12 (2000) 333-337.

[44] G.L. Hansen, J.L. Schmit, T.N.Casselman, Energy gap versus alloy composition and temperature in $Hg_{1-x}Cd_xTe$, J.Appl.Phys 53 (1982) 7099-7101.

[45] A. Ng, C. H. Li, M. K. Fung, A. B. Djurisic, J. A. Zapien, W. K. Chan, K. Y. Cheung, W.-Y. Wong, Accurate determination of the index of refraction of polymer blend films by spectroscopic ellipsometry, J. Phys. Chem. C 114 (2010) 15094-15101.

[46] M. Garriga, M. I. Alonso, C. Domínguez, Ellipsometry on very thick multilayer structures, Phys. Stat. Sol (b) 215, (1999) 247-251.

[47] V. Rinnerbauer, K. Hingerl, M. Kovalenko, W. Heiss, Quantum confinement in layer-by-layer deposited colloidal HgTe nanocrystals determined by spectroscopic ellipsometry, Appl. Surf. Sci. 254 (2007) 291-294.

[48] L. Viña, C. Umbach, M. Cardona, L. Vodopyanov, Ellipsometric studies of electronic interband transitions in $Cd_{1-x}Hg_xTe$, Phys. Rev. B 29 (1984) 6752-6760.

[49] From WVASE reference database "*HgCdTe_comp.mat"* developed by JA Woollam Co partially from data in H. Arwin and D.E. Aspnes, Nondestructive analysis of $Hg_{1-x}Cd_xTe$ (x = 0.00, 0.2, 0.29, and 1.00) by spectroscopic ellipsometry, J. Vac. Sci. Technol. A 2, (1984) 1316-1323.